ELSEVIER

International Journal of Heat and Fluid Flow 20 (1999) 74–83

International Journal of HEAT AND FLUID FLOW

Analysis of heat transfer in a chemical vapor deposition reactor: an eigenfunction expansion solution approach

Hsiao-Yung Chang, Raymond A. Adomaitis *

Department of Chemical Engineering and Institute for Systems Research, University of Maryland, College Park, MD 20742, USA

Received 25 November 1997; accepted 8 August 1998

Abstract

A numerical solution procedure is developed to solve a model for the steady-state gas velocity and temperature distributions in a low-pressure chemical vapor deposition reactor. The gas velocity and three-dimensional temperature fields are both represented in terms of globally defined trial functions; the gas temperature field is discretized using a combined collocation/eigenfunction expansion technique. The enthalpy flux across wafer/gas boundary is calculated explicitly and is found to vary significantly as a function of wafer position. An average heat transfer coefficient is computed from the spatially resolved gas temperature fields and is compared to typical radiative heat transfer rates in these systems. The convergence properties of the discretization method developed are also discussed in the context of quantifying solution accuracy. © 1999 Elsevier Science Inc. All rights reserved.

Keywords: Chemical vapor deposition; Eigenfunction expansions; Weighted residual methods; Collocation

Notation

A_{yz}	the y–z cross sectional area of the gas domain
$a_{lm}, b_{lmn}, c_{lmn}, d_{lmn}, f_{lmn}, g_{lmn}$	mode amplitude coefficients
B, C, G, F	column vectors for coefficients $b_{lmn}, c_{lmn}, g_{lmn}, f_{lmn}$
C_1, C_2	dimensionless variables of gas temperature boundary conditions
C_p	gas mixture heat capacity, J/(kg K)
f, g	representative functions to define inner product
h	average heat transfer coefficient, $J/(\mathrm{m}^2\mathrm{K\ s})$
I	identity matrix
I_i	ith integral
I, J, L, M, N	numbers of modes
$\mathscr{P}$	characteristic pressure drop in x direction, Pa
Q	radiant energy flux, J/(m^2 s)
q	wafer/gas interface energy flux, J/(m^2 s)
$\mathscr{R}$	residual of gas temperature equation
$\mathscr{R}_v$	residual of gas flow equation
R_1	aspect ratio
R_2	radius of susceptor/wafer, m
R_s	susceptor radius, m
R_w	wafer radius, m
r	radial position on wafer
T_{amb}	ambient inlet temperature, K
T_g	gas temperature
$T_{g,z=0}$	gas temperature boundary condition at $z = 0$
T_w	wafer/susceptor temperature
T_{wall}	wall temperature
$T_\Omega, T_{\partial\Omega}$	gas temperature defined by Eq. (4)
t	time
$\langle v \rangle$	average gas flow velocity in chamber, m/s
v_x	gas flow velocity in x direction
v_{max}	maximum gas flow velocity in the chamber, m/s
$\hat{v}_x$	gas flow velocity/pressure drop ratio in x direction
$2\bar{X}, 2\bar{Y}, 2\bar{Z}$	characteristic lengths of gas domain, m
x, y, z	streamwise, spanwise, and normal coordinates
Greek	
α_v, β_v	dimensionless constants of gas momentum balance equation
α_w	dimensionless parameter in wafer energy balance equation $(= R_w^2\epsilon/(\kappa\Delta_z T_{amb}))$
$\beta_{gt}, \gamma_{gt}, \delta_{gt}$	dimensionless constants of gas energy balance equation
ϵ_w	dimensionless parameter in wafer energy balance equation $(= 2\sigma\epsilon R_w^2 T_{amb}^3/(\kappa\Delta_z))$
ζ, ϕ, ψ	trial function components of gas temperature
ζ_0	trial function of gas temperature $(\zeta_0(z = 0) \neq 0)$
η	trial function of gas velocity
κ	gas mixture thermal conductivity, J/(mKs)
$\boldsymbol{\Lambda}$	column vector of eigenvalues
λ	eigenvalues defined by (6)
μ	gas mixture viscosity, kg/(m s)
ξ	normalized trial function of gas velocity

* Corresponding author. E-mail: adomaiti@isr.umd.edu

0142-727X/99/$ – see front matter © 1999 Elsevier Science Inc. All rights reserved.
PII: S 0 1 4 2 - 7 2 7 X (9 8) 1 0 0 4 2 - 5

ρ	gas mixture density, kg/m^3
σ	Boltzmann's constant, J/(m^{2}K^4 s)

Superscripts

$*$	dimensional quantities in SI units

Subscripts

i, j, k, l, m, n	mode numbers

1. Introduction

Chemical vapor deposition (CVD) is a technique extensively used in the semiconductor industry to form nonvolatile solid films on a substrate from chemical reactions fed by the gas phase transport of the reacting species. The quality of the film, e.g., the thickness, composition, and microstructure, is a critical manufacturing requirement. Moreover, the film quality must be reproducible from wafer to wafer and must also be spatially uniform across each wafer.

Temperature, along with pressure, position, and reactant gas composition, is one of the most important factors in high-quality deposition processes. Because the deposition reaction is initiated when the vapor phase reactants receive sufficient energy from the wafer surface or other heat sources, a detailed temperature distribution profile, including the gas phase and wafer, is required for a complete process model. This temperature information also can be used to design and control the reactor to operate at processing conditions that reduce unwanted gas phase reactions which might result in particle contamination.

There is a large literature on the mathematical modeling and simulation of different CVD systems. Kleijn (1995) provides an overview of these modeling issues. Middleman and Hochberg (1993) discuss different modeling aspects from a chemical engineering viewpoint, and Badgwell et al. (1995) summarized modeling and control issues in CVD. Most published CVD system models are solved numerically, either by the finite volume method (Kleijn et al., 1991), finite element method (Moffat and Jensen, 1988), or finite difference method (Duverneuil and Couderc, 1992). These discretization methods are based on spatially localized trial functions, and are well-suited for solving problems with irregular geometries. The large number of algebraic or differential equations that are generated by these discretization procedures, however, may make the resulting simulations inappropriate to use for real-time control applications or iterative optimization methods. On the other hand, those models sufficiently simple to be solved explicitly may be incapable of resolving important physical features.

In this work, we develop an analytical approximation solution based on global trial function expansions to solve a combined set of CVD system gas flow and temperature modeling equations. This choice was motivated by the excellent convergence properties of spectral methods (Gottlieb and Orszag, 1977), and the clear connections that remain during the solution procedure between model parameters and the solution behavior. We see our approach as a method intermediate between the finite element and explicit solution procedures; we feel the techniques presented in this paper are particularly well-suited to distinguishing factors which may require more detailed simulation from those which can be identified as unimportant.

For the CVD system studied, the gas flow field is solved first using a Galerkin projection on a set of globally defined polynomial trial functions. We then use a two-dimensional eigenfunction expansion method, conjugated with a one-point collocation discretization in the spanwise direction, to compute the three-dimensional gas temperature profile. The heat transfer rate at the wafer surface is calculated explicitly from the eigenfunction expansion solution. We compare the contributions of conductive and convective mechanisms to typical radiative heat transfer rates in CVD systems and present a simplified heat transfer coefficient computed by averaging the wafer/gas boundary flux across the wafer.

2. Model formulation

2.1. The CVD system

The BTU-ULVAC ERA-1000 selective tungsten deposition system is the CVD reactor to be considered in this modeling study. The geometry and dimensions of this commercially manufactured, single-wafer, cold-wall reactor are shown in Fig. 1. Reactant gases are fed to the reactor from two sources: a gas mixture of silane, tungsten hexafluoride, and argon carrier gas is injected through a two-dimensional nozzle installed on one side wall, and hydrogen is pumped in through a

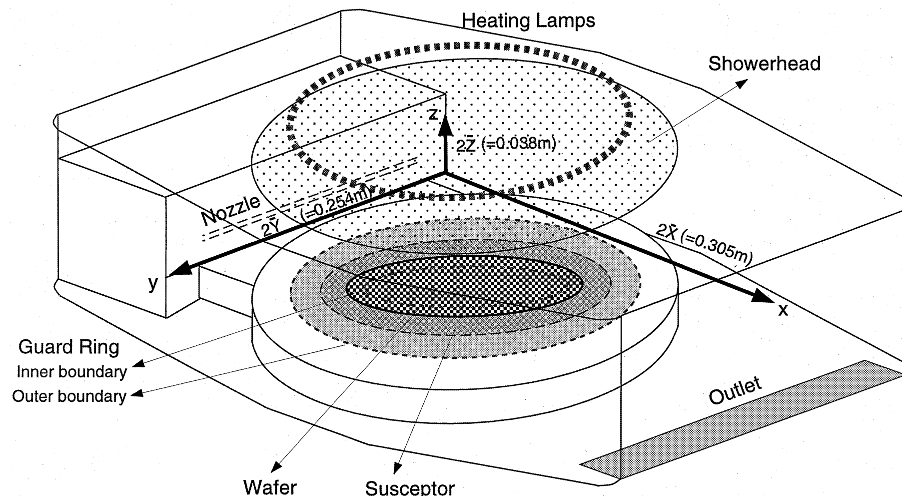

Fig. 1. Sketch of the tungsten CVD reactor system.

transparent showerhead mounted in the top of the reactor chamber. Gases mix in the chamber and react at the surface of a 4 inch wafer located at the chamber center. The wafer is supported by a slowly rotating 0.16 m diameter quartz susceptor and the wafer edge is covered by a quartz guard ring to help reduce edge heat loss. This leaves a 0.076 m diameter area of wafer surface exposed to reaction. An incoherent tungsten–halogen lamp ring is used to heat the wafer to 310°C through the transparent showerhead. Typical deposition runtimes last 5 min after operating temperature is reached.

2.2. Gas flow field

Although feed gas can enter from both the showerhead and side slits, we will only consider the case where the gas flow field over the wafer is assumed to be dominated by the horizontal flow, generated by the feed gas entering through the side wall nozzle. This assumption is suitable in our simulated operating condition in which H_2 is not used; it is also supported by the gas flow visualization tests performed by the system manufacturer (BTU-ULVAC, 1996) using a TiO_2 tracer which demonstrates that a rectangular pipe flow model may be a suitable approximation for the reactant gas mixture in the neighborhood of the wafer. The fully developed, laminar velocity profile is obtained by solving steady state Navier–Stokes and continuity equations. The transport and gas thermodynamic properties are assumed constant and are evaluated at the reference temperature T_{amb}. It is also assumed that the slow wafer rotation as well as buoyancy-induced secondary flows, such as longitudinal and transverse recirculation resulting from free thermal convection near the wafer surface and chamber walls, do not affect the flow field. Since the Grashof number evaluated at the gas inlet is small (Gr = 1.99) in our simulation, transverse recirculations should not occur in this low-pressure system according to the criteria suggested by Ingle and Mountziaris (1994). Other studies, such as Holstein and Fitzjohn (1989) and Jensen (1989), reveal that longitudinal recirculations occur in atmospheric pressure CVD systems at higher Rayleigh numbers (>1780) than those representative of our system (Ra = 1.3463) and so also should not occur. Therefore, the governing equations for the flow field component in the x direction are written as

$$\frac{\partial v_x}{\partial x} = 0,$$

$$\frac{\partial^2 v_x}{\partial y^2} + \alpha_v \frac{\partial^2 v_x}{\partial z^2} = \beta_v.$$

The dimensionless pressure drop term $\beta_v = 2\mathscr{P}\overline{Y}^2/(\mu\langle v\rangle\overline{X})$ can only be determined after the flow field equations are solved. Thus, defining the flow velocity/pressure drop ratio as $\hat{v}_x = v_x/\beta_v$, the momentum balance equation can be written as

$$\frac{\partial^2 \hat{v}_x}{\partial y^2} + \alpha_v \frac{\partial^2 \hat{v}_x}{\partial z^2} = 1, \tag{1}$$

subject to no-slip boundary conditions at $y = 0, 1$ and $z = 0, 1$.

2.3. Gas temperature field

Neglecting heat generated by viscous dissipation and both the gas phase and surface chemical reactions, the gas phase energy balance equation gives

$$v_x \frac{\partial T_{\mathrm{g}}}{\partial x} = \delta_{gt} \frac{\partial^2 T_{\mathrm{g}}}{\partial x^2} + \beta_{gt} \frac{\partial^2 T_{\mathrm{g}}}{\partial y^2} + \gamma_{gt} \frac{\partial^2 T_{\mathrm{g}}}{\partial z^2}. \tag{2}$$

Gas temperature boundary conditions are based on assuming the showerhead temperature equals the chamber wall temperature and that the convective heat transfer dominates at the reactor gas outlet. Gas temperature is set equal to wafer/susceptor temperature T_{w} inside the region of radius R_2 at $z = 0$, and to the wall temperature T_{wall} outside this region:

$$T_{\mathrm{g}} = 0 \quad \text{at } x = 0,$$

$$\frac{\partial T_{\mathrm{g}}}{\partial x} = 0 \quad \text{at } x = 1,$$

$$T_{\mathrm{g}} = C_1(T^*_{\mathrm{wall}}) \quad \text{at } y = 0, 1,$$

$$T_{\mathrm{g}} = C_1(T^*_{\mathrm{wall}}) \quad \text{at } z = 1,$$

$$T_{\mathrm{g}} = \begin{cases} C_2(T^*_{\mathrm{w}}) & \text{at } z = 0,\ (x-0.5)^2 + R_1^2(y-0.5)^2 \leqslant R_2^2, \\ C_1(T^*_{\mathrm{wall}}) & \text{at } z = 0,\ R_2^2 < (x-0.5)^2 + R_1^2(y-0.5)^2. \end{cases} \tag{3}$$

In the above equations, the following dimensionless parameters and variables are used: $x = x^*/2\overline{X}$; $y = y^*/2\overline{Y}$; $z = z^*/2\overline{Z}$; $v_x = v^*_x/\langle v\rangle$; $T_{\mathrm{g}} = (T^*_{\mathrm{g}} - T_{\mathrm{amb}})/T_{\mathrm{amb}}$. Here, T_{amb} is the inlet gas temperature and $\langle v\rangle$ is average gas entrance velocity. Parameters C_1 and C_2 are defined as $(T^*_{\mathrm{wall}} - T_{\mathrm{amb}})/T_{\mathrm{amb}}$ and $(T^*_{\mathrm{w}} - T_{\mathrm{amb}})/T_{\mathrm{amb}}$, respectively. The aspect ratio is $R_1 = \overline{Y}/\overline{X}$ and the radius of the wafer/susceptor is $R_2 = R_{\mathrm{s}}/2\overline{X}$. For the special case where the chamber wall temperature is set equal to constant inlet ambient temperature, the wafer/susceptor becomes the only heat source in the system and $C_1 = 0$, giving homogeneous boundary conditions at all boundaries except $z = 0$.

Representative process operating conditions follow the recipe of Ammerlaan (1994), which correspond to a feed volumetric flow rate of 250 sccm, a feed gas temperature 298 K and mixture ratio of $WF_6/SiH_4/Ar$ equal to 1/1/23, chamber pressure of 0.5 Torr, and a uniform wafer temperature of 310°C. The gas mixture density ρ, thermal conductivity κ, heat capacity C_{p}, and viscosity μ are determined from mixture-averaged properties (Kee et al., 1986) and the pure species viscosities are calculated from the kinetic theory of gases at reference temperature 298 K. The value of dimensionless parameters are given in Table 1.

Table 1
Definitions and values of physical properties and dimensionless parameters

Physical properties [a]	Value	Dimensionless parameters	Value
ρ	0.0013 kg/m^3	$\alpha_v = \overline{Y}^2/\overline{Z}^2$	44.4444
κ	0.0168 J/(m K s)	$\beta_v = 2\mathscr{P}\overline{Y}^2/(\mu\langle v\rangle\overline{X})$	−589.8593
C_{p}	520.19 J/(kg K)	$\alpha_{gt} = \kappa/(\rho C_{\mathrm{p}})$	0.0240
μ	2.18×10^{-5} kg/(m s)	$\delta_{gt} = \alpha_{gt}/(2\langle v\rangle\overline{X})$	0.1203
		$\beta_{gt} = \alpha_{gt}\overline{X}/(2\langle v\rangle\overline{Y}^2)$	0.1732
		$\gamma_{gt} = \alpha_{gt}\overline{X}/(2\langle v\rangle\overline{Z}^2)$	7.6990

[a] All properties are evaluated at reference temperature $T_{\mathrm{amb}} = 298$ K.

3. Flow field solution

A Galerkin technique is used to compute the flow field velocity component $\hat{v}_x$ as a function of y and z. We choose the trial functions η_{ij} to satisfy the no-slip boundary conditions and continuity equation by definition,

$$\eta_{ij} = (y^i - y^{i+1})(z^j - z^{j+1}) \quad i = 1, \ldots, I, \ j = 1, \ldots, J$$

and normalize this sequence with a numerical Gram–Schmidt orthonormalization procedure to define the trial function ξ_{ij}. The residual is formed by substituting the truncated series expansion approximation $\hat{v}_x = \sum_{i,j=1}^{I,J} d_{ij}\xi_{ij}$ into Eq. (1) to obtain

$$\mathscr{R}_v = \sum_{i,j=1}^{I,J} d_{ij}\left(\frac{\partial^2 \xi_{ij}}{\partial y^2} + \alpha_v \frac{\partial^2 \xi_{ij}}{\partial z^2}\right) - 1.$$

The mode amplitude coefficients d_{ij} are computed by minimizing the residual with the Galerkin projection, i.e., projecting the residual onto each trial function ξ_{mn}:

$$\sum_{i,j=1}^{I,J} d_{ij}\left\langle \left(\frac{\partial^2}{\partial y^2} + \alpha_v \frac{\partial^2}{\partial z^2}\right)\xi_{ij}, \xi_{mn}\right\rangle = \langle 1, \xi_{mn}\rangle$$

$$m = 1, \ldots, I, \ \ n = 1, \ldots, J,$$

where the inner product is defined as

$$\langle f, g\rangle = \int_0^1\int_0^1 fg \ \mathrm{d}y\,\mathrm{d}z.$$

The centerline velocity profiles (at $y = 0.5$ and $z = 0.5$) of the two-dimensional flow computed by this procedure are shown in Fig. 2.

The dimensionless parameter β_v and characteristic pressure drop $\mathscr{P}$ can be recovered from the numerically computed solution. Because $v_x^* = \langle v\rangle v_x = \langle v\rangle \beta_v \hat{v}_x$, the volumetric flow rate is found by integrating the dimensionless flow velocity over the unit domain multiplied by the true area of the cross section $A_{yz} = 4\overline{YZ}$:

$$\int_0^{2\overline{Z}}\int_0^{2\overline{Y}} v_x^* \,\mathrm{d}y^*\,\mathrm{d}z^* = 4\overline{YZ}\langle v\rangle\beta_v \int_0^1\int_0^1 \hat{v}_x \,\mathrm{d}y\,\mathrm{d}z.$$

Using the definition of average velocity, $\langle v\rangle = \int_{A_{yz}} v_x^* \,\mathrm{d}y\,\mathrm{d}z / A_{yz}$,

$$\beta_v = \left(\int_0^1\int_0^1 \hat{v}_x \,\mathrm{d}y\,\mathrm{d}z\right)^{-1}$$

$$\mathscr{P} = \frac{\mu\langle v\rangle\overline{X}}{2\overline{Y}^2}\beta_v = 0.0397 \text{ Pa} \quad \text{or} \quad 0.2978 \text{ mTorr}.$$

Under some circumstances this Galerkin procedure generates accurate results with a single term in the series (MacCluer, 1994). This is true in our system in the z direction, but it is not valid in the y direction because of the high aspect ratio α_v of the system; single term versus the converged solutions are compared in Fig. 2. However, since the flow field is essentially flat over the range of y most critical to our heat transfer calculations (the region containing the heated wafer and susceptor), the simplified flow field expression, $v_x(y, z) = 4v_{\max}z(1 - z)$, will be used for the temperature field computations.

4. Gas temperature eigenfunction expansion solution

The first step in computing a solution to the gas temperature model by an eigenfunction expansion technique is to define two separate gas temperature trial function expansions.

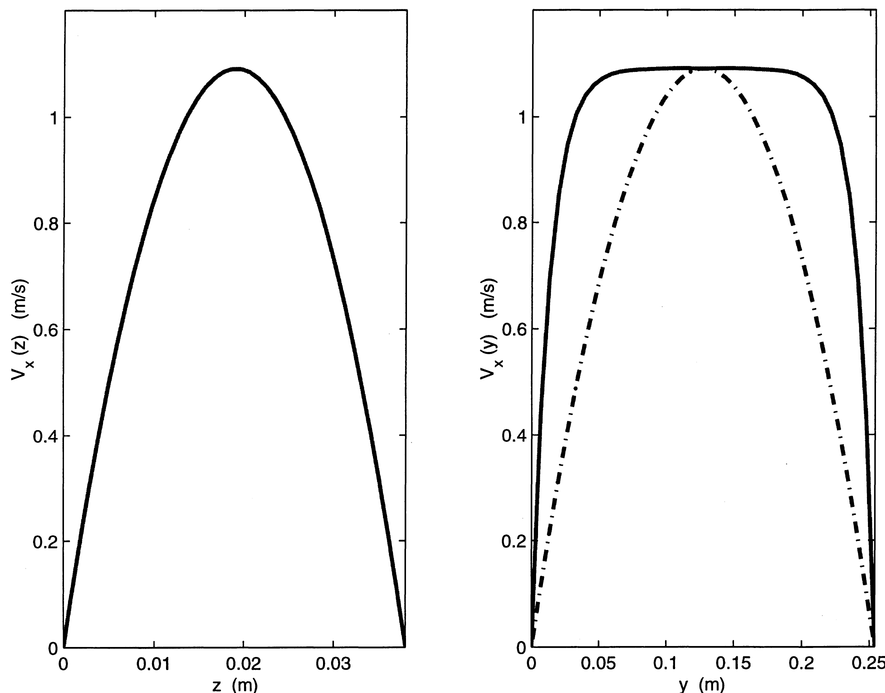

Fig. 2. Comparison of flow field calculations at Re = 1.54 (250 sccm). Solid curves correspond to the $I = J = 16$ term trial function solution. Dashed curves show the single trial function approximation (it lies virtually on top of the solid curve on the left).

The first is used to minimize the temperature equation residual inside the reactor gas domain (T_Ω) and the second expresses the effect of the nonhomogeneous boundary condition on the temperature field ($T_{\partial\Omega}$):

$$T_g = T_\Omega + T_{\partial\Omega}. \tag{4}$$

The trial functions of each series are defined by the product of three individual functions corresponding to each direction of the physical domain shown in Fig. 1

$$T_g = \sum_{l,m,n=1}^{L,M,N} b_{lmn}\phi_l(x)\psi_m(y)\zeta_n(z) + \sum_{l,m,=1}^{L,M,} a_{lm}\phi_l(x)\psi_m(y)\zeta_0(z).$$

In the above equation, b_{lmn} and a_{lm} are mode amplitude coefficients, ϕ_l, ψ_m, and ζ_n are trial function components in the three physical directions, and ζ_0 is chosen to not vanish at $z = 0$.

The solution procedure developed combines collocation discretization in the spanwise (y) direction and an eigenfunction expansion in the (x, z) planes defined at each collocation point y_m. The solution approximately satisfies the governing equation at each collocation position and the three-dimensional results can be reconstructed even when a single interior collocation point is used.

We can write the collocation-discretized trial function expansion as

$$T_g(x, y_m, z) = \psi(y_m)\sum_{l,n=1}^{L,N} b_{lmn}\phi_l(x)\zeta_n(z) + \psi(y_m)\sum_{l=1}^{L} a_{lm}\phi_l(x)\zeta_0(z) \quad m = 1, \ldots, M, \tag{5}$$

where $\psi(y_m)$ is the scalar value of the single trial function ψ at the mth collocation point. The trial function components $\phi(x)$ and $\zeta(z)$ then are computed from the eigenfunctions of the heat equation subject to homogeneous boundary conditions, i.e., solving for nontrivial solutions to

$$\delta_{gt}\frac{\partial^2 T_\Omega}{\partial x^2} + \gamma_{gt}\frac{\partial^2 T_\Omega}{\partial z^2} = -\lambda T_\Omega, \tag{6}$$

where λ is the eigenvalue, subject to boundary condition $T_\Omega = 0$ at $z = 0, 1$ and $x = 0$, and $\partial T_\Omega/\partial x = 0$ at $x = 1$. Applying the separation of variables technique to Eq. (6), the eigenfunctions and eigenvalues are calculated as

$$\phi_l(x) = \sin\left(\frac{2l-1}{2}\pi x\right),$$
$$\zeta_n(z) = \sin(n\pi z),$$
$$\lambda_{ln} = \left[\delta_{gt}\left(\frac{2l-1}{4}\right)^2 + \gamma_{gt}n^2\right]\pi^2, \tag{7}$$

thus, the T_Ω trial function expansion contribution to the temperature field is given by the eigenfunction expansion

$$T_\Omega = \psi(y_m)\sum_{l,n=1}^{L,N} b_{lmn}\sin\left(\frac{2l-1}{2}\pi x\right)\sin(n\pi z).$$

Defining $\zeta_0 = 1 - z$, $T_{\partial\Omega}$ can be represented as

$$T_{\partial\Omega} = \psi(y_m)\sum_{l=1}^{L} a_{lm}\sin\left(\frac{2l-1}{2}\pi x\right)(1-z). \tag{8}$$

The nonhomogeneous boundary condition Eq. (3), denoted as $T_{g,z=0}$, is approximated by projecting the trial function expansion Eq. (8) evaluated at $z = 0$ onto the trial functions $\phi_l(x)$ Eq. (7) to determine the coefficents a_{lm}:

$$\psi(y_m)\sum_{i=1}^{L} a_{im}\int_0^1 \phi_i(x)\phi_l(x)\,dx = \int_0^1 T_{g,z=0}\phi_l(x)dx = \int_{1/2-R_2}^{1/2+R_2} C_2\phi_l(x)\,dx,$$

$$l = 1, \ldots, L$$

to find

$$a_{lm} = \frac{8C_2}{(2l-1)\pi\psi(y_m)}\sin\left(\frac{2l-1}{4}\pi\right)\sin\left(\frac{2l-1}{2}\pi R_2\right).$$

Substituting the trial function expansion Eq. (4) into the heat Eq. (2) defines the residual:

$$\mathscr{R} = \left(\delta_{gt}\frac{\partial^2 T_\Omega}{\partial x^2} + \gamma_{gt}\frac{\partial^2 T_\Omega}{\partial z^2}\right) + \left(\delta_{gt}\frac{\partial^2 T_{\partial\Omega}}{\partial x^2} + \gamma_{gt}\frac{\partial^2 T_{\partial\Omega}}{\partial z^2} - v_x(y,z)\frac{\partial T_{\partial\Omega}}{\partial x}\right) - v_x(y,z)\frac{\partial T_\Omega}{\partial x} + \beta_{gt}\frac{\partial^2 T_\Omega}{\partial y^2} + \beta_{gt}\frac{\partial^2 T_{\partial\Omega}}{\partial y^2}$$

and at the mth collocation point in the y direction

$$\begin{aligned}\mathscr{R}(x, y_m, z) = {} & \sum_{l,n=1}^{L,N} b_{lmn}\psi(y_m)\left(\delta_{gt}\frac{d^2\phi_l}{dx^2}\zeta_n + \gamma_{gt}\phi_l\frac{d^2\zeta_n}{dz^2}\right) \\ & + \sum_{l=1}^{L} a_{lm}\psi(y_m)\left(\delta_{gt}\frac{d^2\phi_l}{dx^2}\zeta_0 - v_x(y_m,z)\frac{d\phi}{dx}\zeta_0\right) \\ & - \sum_{l,n=1}^{L,N} b_{lmn}\psi(y_m)v_x(y_m,z)\frac{d\phi}{dx}\zeta_n + \beta_{gt}\sum_{l,n=1}^{L,N} b_{lmn}\frac{d^2\psi(y_m)}{dy^2}\phi_l\zeta_n \\ & + \beta_{gt}\sum_{l=1}^{L} a_{lm}\frac{d^2\psi(y_m)}{dy^2}\phi_l\zeta_0 \quad m = 1, \ldots, M.\end{aligned} \tag{9}$$

Eigenfunction expansions are used to approximate all nonhomogeneous terms and all terms which are not expressed directly in terms of the eigenfunctions $\phi_l\zeta_n$ defined in Eq. (7). This allows the eigenfunction expansion approximation to the residual to be written as

$$\begin{aligned}\mathscr{R}(x, y_m, z) \approx {} & \psi(y_m)\sum_{l,n=1}^{L,N} b_{lmn}(-\lambda_{ln})\phi_l\zeta_n \\ & - \psi(y_m)\sum_{l,n=1}^{L,N} c_{lmn}\phi_l\zeta_n - \psi(y_m)\sum_{l,n=1}^{L,N} f_{lmn}\phi_l\zeta_n \\ & + \beta_{gt}\frac{d^2\psi(y_m)}{dy^2}\sum_{l,n=1}^{L,N} b_{lmn}\phi_l\zeta_n + \beta_{gt}\frac{d^2\psi(y_m)}{dy^2}\sum_{l,n=1}^{L,N} g_{lmn}\phi_l\zeta_n \\ = {} & \sum_{l,n=1}^{L,N}[\cdots]\phi_l\zeta_n \quad m = 1, \ldots, M.\end{aligned}$$

The mode amplitude coefficients are (for the detailed calculations, see Appendix A)

$$c_{lmn} = \frac{\delta_{gt}\pi}{2n}(2l-1)^2 a_{lm} + \frac{8v_{\max}}{n^3\pi^3} a_1(1-(-1)^{2l-1})(2+(-1)^n)a_{lm} + \frac{8v_{\max}}{n^3\pi^3}(2+(-1)^n)\sum_{\substack{j=1\\ j\neq l}}^{L} a_{jm}(2j-1) \times \left(\frac{1-(-1)^{l+j-1}}{l+j-1} + \frac{1-(-1)^{l-j}}{l-j}\right),$$

$$f_{lmn} = 8v_{\max}\left(\frac{1}{3}+\frac{1}{n^2\pi^2}\right)b_{lmn} + 16\frac{v_{\max}}{\pi^2}\sum_{j}^{L}\sum_{\substack{k=1\\ k\neq n}}^{N} b_{jmk} \times \left(\frac{1+(-1)^{k+n}}{(k+n)^2} - \frac{1+(-1)^{k-n}}{(k-n)^2}\right) + 4v_{\max}\left(\frac{1}{3}+\frac{1}{n^2\pi^2}\right) \times (2l-1)\sum_{\substack{j=1\\ j\neq l}}^{L}\sum_{k=1}^{N} b_{jmk}\left(\frac{1-(-1)^{l+j-1}}{l+j-1} + \frac{1-(-1)^{l-j}}{l-j}\right) + 8\frac{v_{\max}}{\pi^2}\sum_{\substack{j=1\\ j\neq l}}^{L}\sum_{\substack{k=1\\ k\neq n}}^{N} b_{jmk}(2j-1)\left(\frac{1-(-1)^{l+j-1}}{l+j-1} + \frac{1-(-1)^{l-j}}{l-j}\right) \times \left(\frac{1+(-1)^{k+n}}{(k+n)^2} - \frac{1+(-1)^{k-n}}{(k-n)^2}\right),$$

$$g_{lmn} = \frac{2}{n\pi} a_{lm}.$$

Projecting the residual approximation onto each trial function $\phi_l\zeta_n$ and setting the resulting equation to zero gives,

$$\left(\psi(y_m)\lambda_{ln} - \beta_{gt}\frac{d^2\psi(y_m)}{dy^2}\right)b_{lmn} + \psi(y_m)\sum_{j,k=1}^{L,N} b_{jmk}I_5I_6 = -\psi(y_m)c_{lmn} + \beta_{gt}\frac{d^2\psi(y_m)}{dy^2}g_{lmn} \quad l=1,\ldots,L,\ n=1,\ldots,N,$$

where f_{lmn} is replaced by $\sum_{j,k=1}^{L,N} b_{jmk}I_5I_6$, and I_5, I_6 are defined in Appendix A.

A computationally efficient method for calculating the b_{lmn} is to rearrange each $b_{lmn}, c_{lmn}, g_{lmn}$, and λ_{ln} array into column vector format $\mathbf{B},\mathbf{C},\mathbf{G},\ \mathbf{\Lambda}$, respectively, and to reorder the fourth-order tensor, generated by the product of I_5 and I_6, into an array $\mathbf{F}$. This gives

$$\left[\mathbf{I}\left[\psi(y_m)\mathbf{\Lambda} - \beta_{gt}\frac{d^2\psi(y_m)}{dy^2}\right] + \psi(y_m)\mathbf{F}\right]\mathbf{B} = -\psi(y_m)\mathbf{C} + \beta_{gt}\frac{d^2\psi(y_m)}{dy^2}\mathbf{G}, \tag{10}$$

where $\mathbf{I}$ is identity matrix. Since there are $L \times M \times N$ unknown b_{lmn} coefficients and $L \times M \times N$ equations, this linear system can be solved directly to find gas phase temperature, given the flow field characteristic $v_{\max}$ and wafer/susceptor and ambient gas temperatures used to compute C_2.

5. Results and discussions

Based on the preceding analysis, representative results are presented for the computed gas temperature profile at the centerline of the reactor chamber when the trial function ψ in the y direction is selected as $4y(1-y)$. This corresponds to $M = 1$ and $y_1 = 0.5$.

5.1. Solution convergence

The error of the eigenfunction expansion solution results from the truncated, finite-term expansions of both the nonhomogeneous boundary condition and the eigenfunction expansion approximation of all terms in the gas temperature residual not expressed directly in terms of the eigenfunctions. The modal nature of eigenfunction expansion-based discretization techniques means that the values of the coefficients b_{lmn} and a_{lm} do not depend on the truncation number L and N. Therefore, the magnitude of the L_2 norm of the residual defined by substituting the truncated trial function expansion into Eq. (2) can be estimated by computing the rates of decrease of b_{lmn} and a_{lm} magnitudes as l, n approach infinity. Figs. 3 and 4 display the magnitudes of these mode amplitude coefficients. The decreasing amplitude in a_{lm} and b_{lmn} for increasing mode numbers is a strong indicator of the trial function expansion convergence in an L_2-norm sense. We note that the relative rates of convergence (i.e., modes l versus modes n) in the expansion coefficients b_{lmn} are governed by the eigenvalues λ_{ln}, where an inverse relationship is observed between the magnitudes of eigenvalues and the mode coefficients

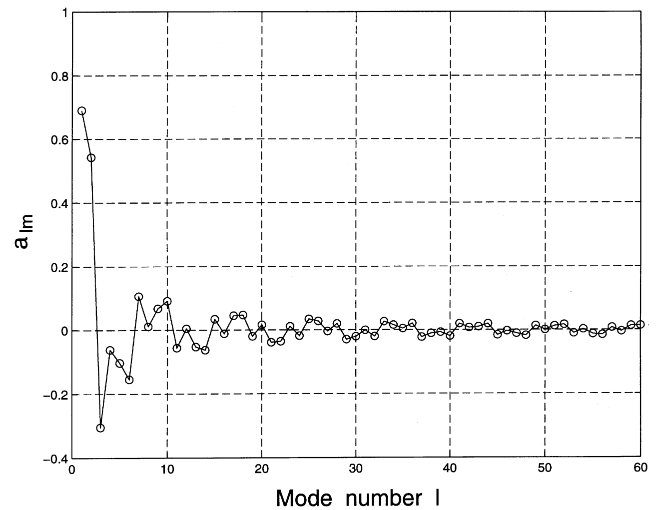

Fig. 3. The boundary mode amplitude coefficients a_{lm}.

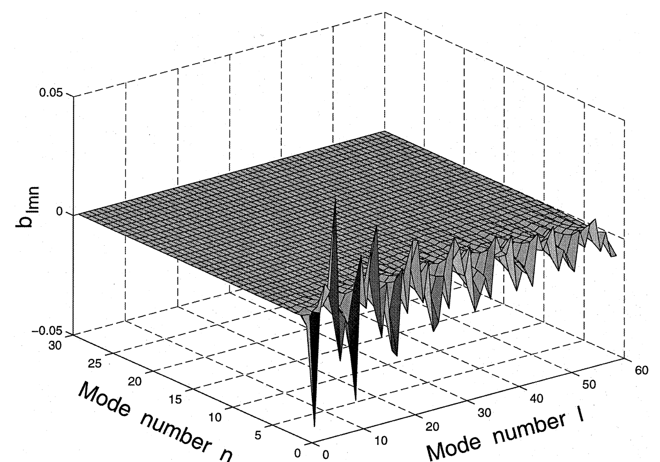

Fig. 4. The interior mode amplitude coefficients b_{lm}.

when solving the linear system Eq. (10). Furthermore, as represented in Eq. (7), the eigenvalue magnitude depends more strongly on mode number n relative to l because the dimensionless parameter γ_{gt} is much larger than δ_{gt}. These different contributions to eigenvalue growth rate results in the amplitudes b_{lmn} becoming small after only several modes of n, requiring a larger total mode number L relative to N to achieve a "balanced" convergence behavior in the x and z directions.

5.2. Gas temperature and Gibbs phenomenon

A representative gas temperature field solution is presented in Fig. 5; the thick contour lines are reconstructed directly from Eq. (5). The Gibbs phenomenon (Gottlieb and Orszag, 1977) results from the discontinuities in the piecewise-smooth gas temperature boundary condition at $z = 0$, and is most prominent near the wafer leading and trailing edges. *It is important to stress that these wiggles are a true feature of the solution*, and are an indicator of convergence of global trial functions near the discontinuities. As reported in a recent paper of Gottlieb and Shu (1997), the global nature of the Fourier series, where the Fourier mode coefficients are determined by integration over the *entire* domain including the discontinuities, contributes to the slow decay of the mode amplitude coefficients as seen in Figs. 3 and 4 associated with the modes $\phi_l(x)$. One approach to enhancing the convergence rate for a given set of Fourier coefficients is to use Fourier-space filters, which eliminate the truncation error resulting from the finite Fourier sum (Gottlieb and Shu, 1997). There are no additional computational costs associated with using this filter, and filtered results converge to the same solution as unfiltered profiles in an L_2 sense. Two, second-order filters $\sigma_\Omega(l,n)$ and $\sigma_{\partial\Omega}(l)$ based on the cosine function are used for the post-processing reconstruction of the gas temperature profile:

$$T_g(x,y_m,z) = \psi(y_m)\sum_{l,n=1}^{L,N} b_{lmn}\sigma_\Omega(l,n)\phi_l(x)\zeta_n(z) + \psi(y_m)\sum_{l=1}^{L} a_{lm}\sigma_{\partial\Omega}(l)\phi_l(x)\zeta_0(z), \quad m = 1,\ldots,M,$$

$$\sigma_\Omega(l,n) = \frac{1}{4}\left(1+\cos\left(\frac{\pi l}{L}\right)\right)\left(1+\cos\left(\frac{\pi n}{N}\right)\right)$$

$$\sigma_{\partial\Omega}(l) = \frac{1}{2}\left(1+\cos\left(\frac{\pi l}{L}\right)\right).$$

The thin contour lines in Fig. 5 correspond to the filtered results, demonstrating how the oscillations associated with the Gibbs phenomenon are removed from the contours. Minor deviations occur near the wafer leading edge and the trailing edge because of the nature of the Fourier-space filter, which tends to increase the convergence rate inside the piecewise smooth segments and smooth the solutions in the neighborhood of the discontinuities. Increasing the number of trial functions reduces these deviations since both filtered and unfiltered results converge to the same solution.

Fig. 6 shows the comparison of two filtered temperature profiles computed for the nominal feed gas flow rate of 250 sccm and a case corresponding to 2500 sccm. From the temperature contour lines in (a), it is observed that convective effects appear to contribute little to the energy transferred from the wafer to gas phase over conduction, giving a large, high-temperature area in the region above and slightly downstream of the wafer. At ten times of the nominal flow, as shown in (b), the temperature contours show the apparent distortion of the heated gas profile due to the convective transport of thermal energy out of the heated gas zone. Heat transfer rates at the top wafer surface, defined as the heat flux from wafer to the adjacent reactant gas, are shown in Fig. 6(c)–(d). The heat transfer rates as a function of wafer position can be computed by evaluating the derivatives of the gas temperature at $z = 0$

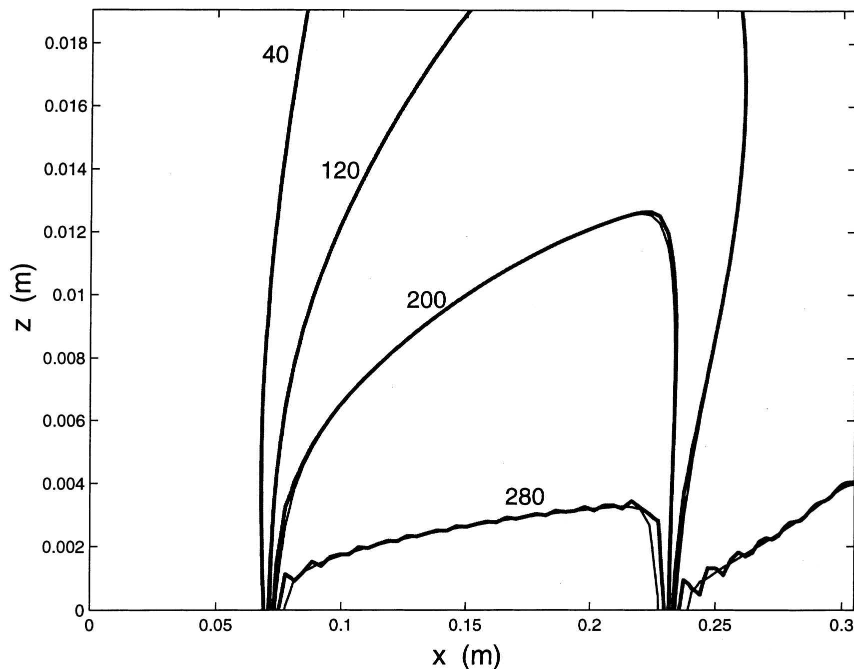

Fig. 5. Comparison of filtered and unfiltered gas temperature fields. The dark contour lines show the Gibbs phenomenon near the wafer surface particularly near the leading and trailing edges. The light contour lines are filtered by a Fourier-space filter.

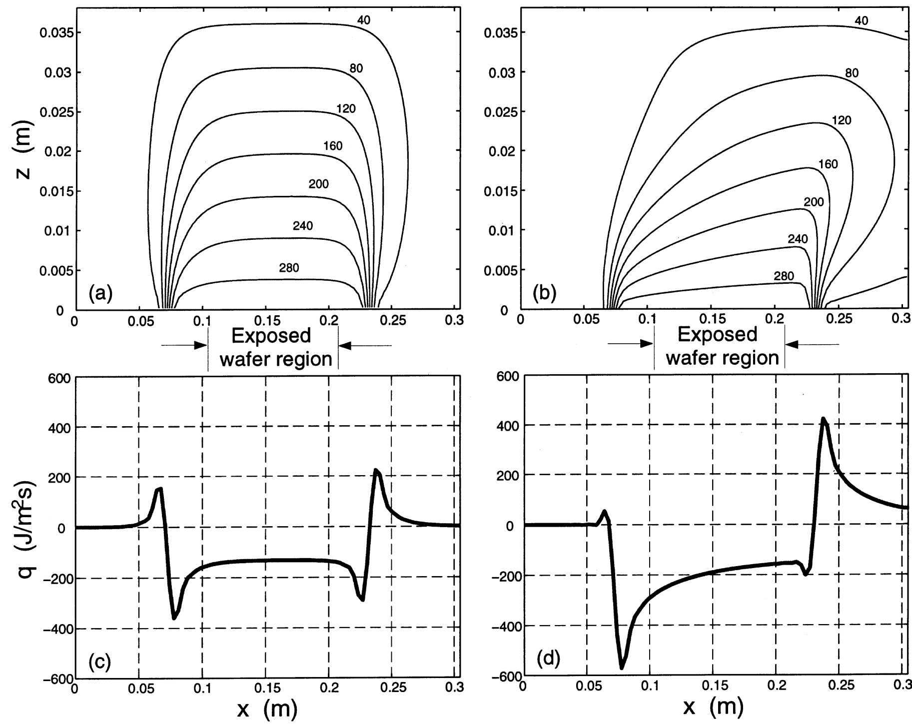

Fig. 6. Gas temperature solution and wafer/gas heat transfer rates at centerline of the reactor chamber with different gas flow velocities. Temperature contour lines are labeled in °C. (a), (c) Simulation performed at Re = 1.54 (250 sccm). (b), (d) Simulation performed at Re = 15.36 (2500 sccm).

$$q(x,y) = \kappa\left(\frac{\partial T_g^*}{\partial z^*}\right)_{z=0} = \kappa\frac{T_{amb}}{2\overline{Z}}\left(\frac{\partial}{\partial z}(T_\Omega + T_{\partial\Omega})\right)_{z=0}$$
$$= \kappa\frac{T_{amb}}{2\overline{Z}}\psi(y_m)\left(\sum_{l,n=1}^{L,N} b_{lmn} n\pi \sin\left(\frac{2l-1}{2}\pi x\right) - \sum_{l=1}^{L} a_{lm}\sin\left(\frac{2l-1}{2}\pi x\right)\right). \quad (11)$$

In Fig. 6(c)–(d) we observe that the enthalpy flux at $z = 0$ is nearly zero over the range of x from the gas inlet to the wafer leading edge. The amount of energy exchanged suddenly jumps to its maximum value when gas crosses the wafer leading edge. As the gas temperature near the wafer increases, the heat transfer rate slows. After the gas passes the wafer trailing edge, the high temperature gas exchanges energy back to the low temperature chamber wall and results in a positive transfer rate. The enthalpy flux plots show the increased heat transfer at higher gas velocity, since convection enhances the total energy transfer.

5.3. Comparison to radiative heat transfer rates

In a previous study (Adomaitis, 1997), a wafer thermal dynamics model was developed which accounted for radiative heat exchange between the wafer and chamber walls, heating from the lamp banks, and thermal conductivity through the wafer being processed:

$$\frac{\partial T_w}{\partial t} = \frac{1}{r}\frac{\partial}{\partial r}\left(r\frac{\partial T_w}{\partial r}\right) + \epsilon_w(1 - T_w^4) + \alpha_w Q.$$

The dimensionless wafer temperature is defined as $T_w = T_w^*/T_{amb}$, radial position $r = r^*/R_w$, and time $t = kt^*/\rho C_p R_w^2$. At steady state, and for uniform wafer temperature and vacuum conditions, the wafer temperature equation can be used to determine the energy loss by radiation because the energy provided by the heating lamp will balance radiative energy loss. Assuming a spatially uniform lamp radiant energy distribution and substituting the process parameters into the equation, the radiant energy flux required to maintain a wafer at 310°C is

$$Q = 2\sigma T_{amb}^4(T_w^4 - 1) = 12,221 \quad \mathrm{J/(m^2 s)},$$

where σ is the Boltzmann's constant $= 5.677 \times 10^{-8}$ $\mathrm{J/(m^2K^4s)}$. Comparing this result with the heat transfer rate plotted in Fig. 6(c), we conclude that gas/wafer heat transfer accounts for only about 1% of the wafer energy loss in this low-pressure system. However, because of the large volume of heated gas above the wafer, our analysis alerts us to the possibility of gas phase reactions in this process.

5.4. Average heat transfer coefficient

Another application of our solution approach is the numerical estimation of an average heat transfer coefficient h, which usually is estimated by collecting experimental data and determining correlations on the basis of dimensional analysis. The heat exchange relation we wish to find has the following form

$$h(T_{amb} - T_w^*) = \kappa\left(\frac{\partial T_g^*}{\partial z^*}\right)_{z=0}.$$

The total energy transferred from wafer to gas phase is calculated by integrating the right-hand side of this equation obtained from Eq. (11) over the wafer surface. The average heat transfer coefficient is obtained by dividing the total energy with the wafer-feed gas temperature difference and the wafer surface area. The relationship of h and Reynolds number is plotted in Fig. 7. Comparing the heat transfer coefficient at zero gas flow with the value obtained at the nominal operating

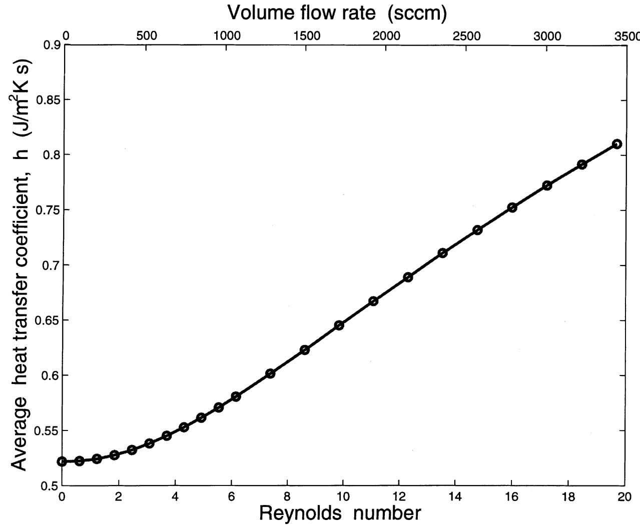

Fig. 7. The relationship of Reynolds number and average heat transfer coefficient h at 0.5 Torr.

condition (Re = 1.54), we find further evidence that convective transport effects contribute little to overall heat transfer under normal operating conditions for this CVD processing recipe.

6. Concluding remarks

In this paper, a hybrid weighted residual method for computing solutions to the gas flow and temperature fields was developed and applied to a commercial CVD reactor system. The solution procedure developed allows fast and demonstratively accurate analysis of models whose complexity lies in between those that can be solved analytically and those that must be solved with finite element packages. We believe one of the primary benefits of this approach is its utility in distinguishing factors which warrant more detailed analysis from those which do not.

Using the procedure developed, the heat transfer rate was calculated explicitly at the wafer/gas boundary. A comparison between the convective heat loss of the wafer with the radiative energy losses showed clearly that convective heat transfer only has small effect in this low-pressure system. A heat transfer coefficient was estimated from the global trial function expansion solution by integrating the heat flux across the wafer. The convergence of the solution was demonstrated by the decreasing mode amplitude coefficients of the eigenfunction expansion solution.

Acknowledgements

This work was supported by the National Science Foundation through grant NSF EEC 95-27 576 and the Petroleum Research Fund of the American Chemical Society through grant 31391-G9.

Appendix A

The unknown coefficients c_{lmn}, f_{lmn}, and g_{lmn} can be found by multiplying both sides of the corresponding equations listed below by $\phi_l\zeta_n$ and integrating over the unit domain.

1. $\psi(y_m)\sum_{j,k=1}^{L,N} c_{jmk}\phi_j\zeta_k = \psi(y_m)\sum_{j=1}^{L} a_{jm}(-v_x(\mathrm{d}\phi_j/\mathrm{d}x)\zeta_0 + \delta_{gt}(\mathrm{d}^2\phi_j/\mathrm{d}x^2)\zeta_0)$

$$c_{lmn} = 4\sum_{j=1}^{L} a_{jm}\left[\left(\frac{2j-1}{2}\right)\pi\int_0^1 \cos\left(\frac{2j-1}{2}\pi x\right) \times \sin\left(\frac{2l-1}{2}\pi x\right)\mathrm{d}x\right]\left[4v_{\max}\int_0^1 z(1-z)^2\sin(n\pi z)\mathrm{d}z\right]$$

$$+4\sum_{j=1}^{L} a_{jm}\left[\left(\frac{2j-1}{2}\right)^2\pi^2\delta_{gt}\int_0^1 \sin\left(\frac{2j-1}{2}\pi x\right) \times \sin\left(\frac{2l-1}{2}\pi x\right)\mathrm{d}x\right]\left[\int_0^1 (1-z)\sin(n\pi z)\mathrm{d}z\right]$$

$$= 4\sum_{j=1}^{L} a_{jm}I_1I_2 + 4\sum_{j=1}^{L} a_{jm}I_3I_4$$

$$l = 1,\ldots,L,\quad m = 1,\ldots,M,\quad n = 1,\ldots,N$$

and the four integrals are calculated as follows.

$$I_1 = \left(\frac{2j-1}{2}\right)\pi\int_0^1 \cos\left(\frac{2j-1}{2}\pi x\right)\sin\left(\frac{2l-1}{2}\pi x\right)\mathrm{d}x$$

$$= \begin{cases} \frac{1-(-1)^{2l-1}}{4} & \text{if } j = l, \\ \frac{(2j-1)}{4}\left(\frac{1-(-1)^{l+j-1}}{l+j-1} + \frac{1-(-1)^{l-j}}{l-j}\right) & \text{if } j \neq l, \end{cases}$$

$$I_2 = 4v_{\max}\int_0^1 z(1-z)^2\,\sin(n\pi z)\mathrm{d}z = \frac{8v_{\max}}{n^3\pi^3}(2+(-1)^n),$$

$$I_3 = \left(\frac{2j-1}{2}\right)^2\pi^2\delta_{g_t}\int_0^1 \sin\left(\frac{2j-1}{2}\pi x\right)\sin\left(\frac{2l-1}{2}\pi x\right)\mathrm{d}x$$

$$= \begin{cases} \frac{1}{2}\left(\frac{2l-1}{2}\right)^2\pi^2\delta_{g_t} & \text{if } j = l, \\ 0 & \text{if } j \neq l, \end{cases}$$

$$I_4 = \int_0^1 (1-z)\sin(n\pi z)\mathrm{d}z = \frac{1}{n\pi},$$

2. $\psi(y_m)\sum_{j,k=1}^{L,N} f_{jmk}\phi_j\zeta_k = \psi(y_m)\sum_{j,k=1}^{L,N} b_{jmk}v_x(\mathrm{d}\psi_j/\mathrm{d}x)\zeta_k$

$$f_{lmn} = 4\sum_{j,k=1}^{L,N} b_{jmk}\left[\int_0^1\left(\frac{2j-1}{2}\right)\pi\cos\left(\frac{2j-1}{2}\pi x\right)\sin\left(\frac{2l-1}{2}\pi x\right)\mathrm{d}x\right] \times \left[4v_{\max}\int_0^1 z(1-z)\sin(k\pi z)\sin(n\pi z)\,\mathrm{d}z\right]$$

$$= \sum_{j,k=1}^{L,N} b_{jmk}I_5I_6 \quad l = 1,\ldots,L,\quad m = 1,\ldots,M,\quad n = 1,\ldots,N$$

and

$$I_5 = 4\int_0^1 \left(\frac{2j-1}{2}\right)\pi \cos\left(\frac{2j-1}{2}\pi x\right) \sin\left(\frac{2l-1}{2}\pi x\right) \mathrm{d}x = \begin{cases} 2 & \text{if } j = l, \\ (2j-1)\left(\frac{1-(-1)^{l+j-1}}{l+j-1} + \frac{1-(-1)^{l-j}}{l-j}\right) & \text{if } j \neq l, \end{cases}$$

$$I_6 = 4v_{\max}\int_0^1 z(1-z)\sin(k\pi z)\sin(n\pi z)\mathrm{d}z = \begin{cases} 4v_{\max}\left(\frac{1}{12}+\frac{1}{4n^2\pi^2}\right) & \text{if } k = n, \\ \frac{2v_{\max}}{\pi^2}\left(\frac{1+(-1)^{k+n}}{(k+n)^2} - \frac{1+(-1)^{k-n}}{(k-n)^2}\right) & \text{if } k \neq n, \end{cases}$$

3. $(\mathrm{d}^2\psi(y_m)/\mathrm{d}y^2)\sum_{j,k=1}^{L,N} g_{jmk}\phi_j\zeta_k = (\mathrm{d}^2\psi(y_m)/\mathrm{d}y^2)\sum_{j=1}^{L} a_{jm}\phi_j\zeta_0$

$$g_{lmn} = 4\sum_{j=1}^{L} a_{jm}\left[\int_0^1 \sin\left(\frac{2j-1}{2}\pi x\right)\sin\left(\frac{2l-1}{2}\pi x\right)\mathrm{d}x\right] \times \left[\int_0^1 (1-z)\sin(n\pi z)\mathrm{d}z\right] = \begin{cases} \frac{2}{n\pi}a_{lm} & \text{if } j = l, \\ 0 & \text{if } j \neq l, \quad l = 1,\ldots,L, \quad m = 1,\ldots,M, \quad n = 1,\ldots,N \end{cases}$$

References

Adomaitis, R.A., 1997. An orthogonal collocation technique for rapid thermal processing system discretization. Institute for Systems Research, University of Maryland, College Park. Technical Report TR97–63.

Ammerlaan, J.A.M., 1994. Kinetics and characterization of Tungsten CVD processes. Delft University Press, Netherlands, pp. 64–71.

Badgwell, T.A., Breedijk, T., Bushman, S.G., Butler, S.W., Chatterjee, S., Edgar, T.F., Toprac, A.T., Trachtenberg, I., 1995. Modeling and control of microelectronics materials processing. Computers Chem. Eng. 19, 1–41.

BTU-ULVAC Inc., 1996. BTU-ULVAC ERA-1000 Selective Tungsten Deposition System. North Billerica, MA.

Duverneuil, P., Couderc, J.P., 1992. Two-dimensional modeling of low-pressure chemical vapor deposition hot wall tubular reactor. J. Electrochem. Soc. 139, 296–304.

Gottlieb, D., Orszag, S.A., 1977. Numerical Analysis of Spectral Methods: Theory and Applications. Society for Industrial and Applied Mathematics, Philadelphia, pp. 155–157.

Gottlieb, D., Shu, C.-W., 1997. On the Gibbs phenomena and its resolution. SIAM Review 39, 644–668.

Holstein, W.L., Fitzjohn, J.L., 1989. Effect of buoyancy forces and reactor orientation of fluid flow and growth rate uniformity in cold-wall channel CVD reactors. J. Crystal Growth 94, 145–158.

Ingle, N.K., Mountziaris, T.J., 1994. The onset of transverse recirculations during flow of gases in horizontal ducts with differentially heated lower walls. J. Fluid Mech. 277, 249–269.

Jensen, K.F., 1989. Transport phenomena and chemical reaction issues in OMUPE of compound semiconductors. J. Crystal Growth 98, 148–166.

Kee, R.J., Dixon-Lewis, G., Warnatz, J., Coltrin, M.E., Miller, J., 1986. A FORTRAN computer code package for the evaluation of gas-phase multicomponent transport properties. Sandia National Laboratories, Albuquerque/Livermore, Technical Report SAND86–8246.

Kleijn, C.R., 1995. Chemical vapor deposition processes. In: Meyyappan, M. (Ed.), Computational Modeling in Semiconductor Processing. Artech House, Boston, pp. 97–229.

Kleijn, C.R., Hoogendoorn, C.J., Hasper, A., Holleman, J., Middelhoek, J., 1991. Transport phenomena in tungsten LPCVD in a single-wafer reactor. J. Electrochem. Soc. 138, 509–517.

MacCluer, C.R., 1994. Boundary Value Problems and Orthogonal Expansions. IEEE Express, New York, pp. 290–292.

Middleman, S., Hochberg, A., 1993. Process Engineering Analysis in Semiconductor Device Fabrication. McGraw-Hill, New York, pp. 478–573.

Moffat, H.K., Jensen, K.F., 1988. Three-dimensional flow effects in silicon CVD in horizontal reactors. J. Electrochem. Soc. 135, 459–471.